ICAS 2021 SHANGHAI
International Council of the Aeronautical Sciences
32nd Congress of the International Council of the Aeronautical Sciences
September 6-10, 2021
Pudong Shangri-La, Shanghai, China

NUMERICAL SIMULATION ON AERODYNAMIC PERFORMANCE OF BIRD-LIKE FLAPPING WING LEADING EDGE COVERTS

Jiangxin Gao[1], Wenqing Yang[1,2], Rui Zhang[1], Yuanbo Li[1]

[1]School of Aeronautics, Northwestern Polytechnical University, Xi'an, 710072, P. R. China

[2]Research & Development Institute of Northwestern Polytechnical University in Shenzhen, Shenzhen, 518057, China

Abstract

In order to further improve the flight efficiency of bionic Flapping-wing micro air vehicles (FMAVs), a bionic leading edge device was proposed according to the structure of leading edge feathers of birds, inspired by the changes of wings during take-off and landing, and its numerical simulation was carried out.At a Reynolds number of 1.0×10^5, the aerodynamic force and flow field of NACA0012 airfoil with a leading edge device were analyzed.The leading edge device is a circular spoiler near the leading edge of an airfoil.In this paper, the leading edge devices with different geometrical parameters are numerically simulated at $5°$ and $15°$ angles of attack. It is found that the effect of leading edge devices is not obvious at small angles of attack.At high Angle of attack, the leading edge device at certain deflection Angle has obvious lift, drag and lift to drag ratio improvement.The findings also support previous speculation that leading edge feathers increase lift and drag during takeoff and landing.

Keywords: flapping wing, bionics, leading edge coverts, leading edge devices, leading edge flaps

1. Introduction

The flying creatures in nature have strong flying ability and adaptability to the environment, while the birds that can fly flexibly arouse people's strong interest.Different birds have different flight modes, some can achieve high maneuvering flight, some can achieve long distance and endurance flight, some can maintain continuous hovering. These varied flight modes attract the attention of many researchers.It also gave birth to the research on Flapping-wing micro air vehicles (FMAVs).Many studies are inspired by birds, and these inspirations are also well used in the research and design process of flapping wing aircraft.Compared with the flying creatures in nature, the flying ability of bionic flapping wing aircraft is still very clumsy, and there is still a large distance from high bionic, especially in the take-off and landing stage.

Since the 1970s, researchers have been studying the structural characteristics of bird wings, finding that they can adapt to a variety of different structures, from the relatively rigid geometry of gliding to the highly flexible kinematics of flapping.During take-off, landing, and maneuvering, the wings must maintain control at high angles of attack and generate highly unsteady flow.The experiment by Carruthers et al[1,2]. recorded the aeroelastic devices on the wings of prairie eagles during manoeuvring with high-speed cameras and found that the lower surface leading edge coverts automatically deflects along the leading edge at high angles of attack and can be used as a increase lift device similar to Krueger flaps[5,6,7].As shown in Figure 1, leading edge coverts deflects greatly during bird flight and landing.It has been observed that when birds fly at high angles of attack, such as take-off and landing, the leading edge small covert feathers of under the wing surface will deflect greatly.Small coverts can also deflect if they are affected by gusts during cruising flight.

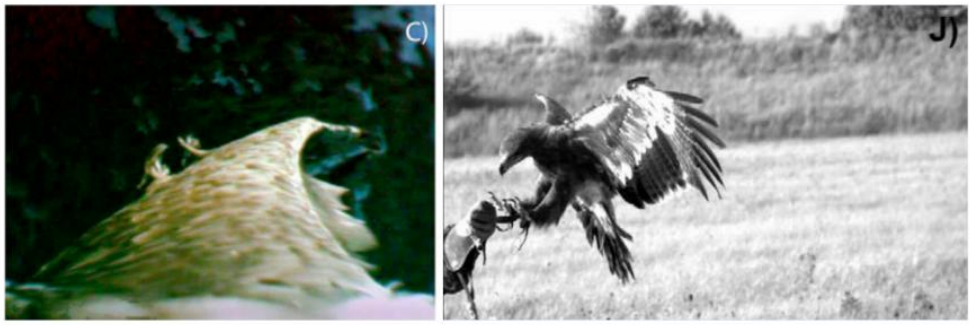

Figure 1- The leading edge coverts of birds during flight and landing

Jones et al[3,4]. Believe that the leading edge coverts is a high lift device, which can improve the lift at low Reynolds number and high angle of attack. When the wing is at high angle of attack, it will expand automatically, as shown in Figure 2. At Reynolds number from 4.0×10^4 to1.2×10^5 ,The leading edge devices such as leading edge wire and leading edge flap mounted on the Eppler E423 airfoil were used to measure the force and study the flow visualization. As shown in Figure 3, it is found that the leading edge device is only effective at high angles of attack, and its characteristic is that the lift increases suddenly at some critical angles of attack. Larger flap deflection delays the increase of lift to a higher angle of attack.

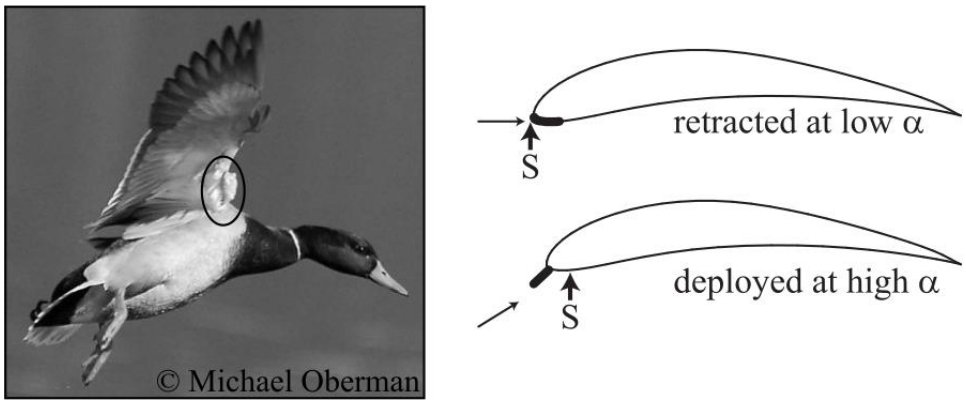

Figure 2 - The leading edge flap is deployed automatically. At a certain angle of attack, the stagnation point S moves to the rear of the flap, resulting in the flap deployment

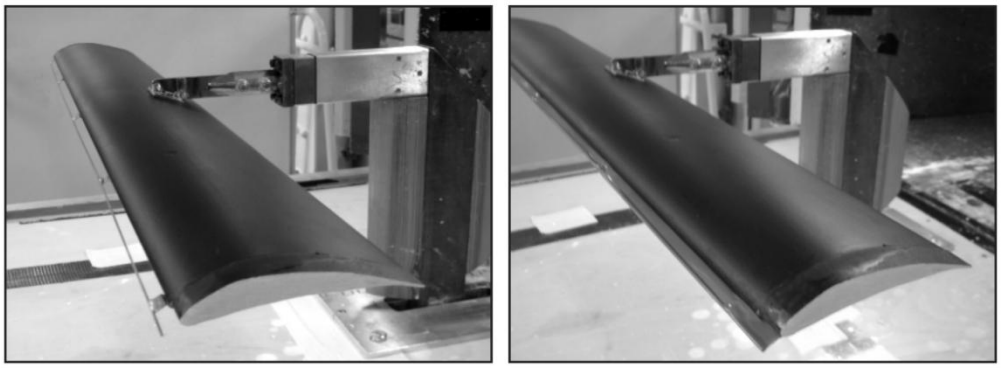

Figure 3 - Installation of leading edge device

In this paper, based on the research of Jones et al., the numerical simulation of the wire shaped leading edge device is carried out. The research goal is to understand the aerodynamic mechanism of the leading edge device producing high lift and to explore the design of the leading edge device, especially the influence of the deflection angle on the effectiveness of the device.

2. Model Settings and Methods

2.1 Model setup

In order to study the influence of leading edge devices with different geometric parameters on airfoil aerodynamic performance, a two-dimensional numerical simulation model was established. Because the leading edge coverts exists in the leading edge of the bird's inner wing (arm wing), and the three-dimensional flow effect of the bird's inner wing is not obvious, the flapping and twisting motion of the inner wing can be simplified as two-dimensional plunging and pitching motion. The purpose of this paper is to study the influence of leading edge device on the aerodynamic performance of airfoil, so NACA0012 symmetric airfoil is used as the main airfoil. The plunging and pitching motion law of the airfoil is shown in equation (1)and (2).

$$\alpha(\mathrm{t}) = \alpha_0 + \alpha_m \cos(2\pi f t + \pi/2) \tag{1}$$

$$h(t) = h_m \cos(2\pi f t) \tag{2}$$

Where $\alpha(\mathrm{t})$ is the instantaneous pitching Angle; α_0 is the Angle of attack of free incoming flow; α_{m} is the pitch range; $\mathrm{h}(t)$ is the instantaneous plunging displacement, h_{m} is the plung amplitude, f is the flapping frequency.The pitching axis is 1/4 chord length from the leading edge, and the airfoil movement is shown in Figure 4.

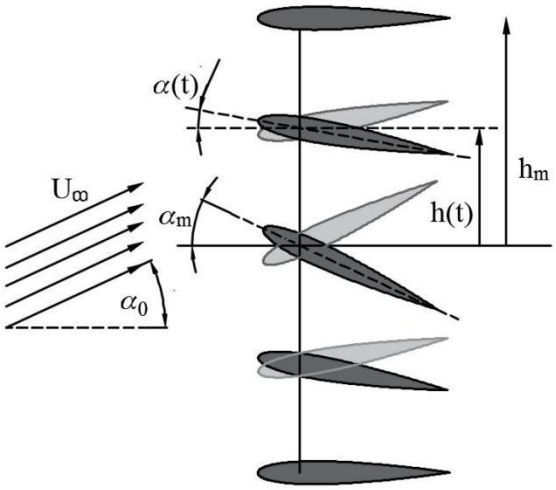

Figure 4 - two dimensional airfoil pitching, plunging motion diagram
(dark color: up stroke; light color: down stroke)

The drag (D) of the airfoil is in the same direction as the free flow, the lift (L) is perpendicular to the drag, the lift coefficient and drag coefficient are calculated by equation (3), and the time average lift coefficient and time average drag coefficient are calculated by equation (4). The setting of relevant calculation parameters is shown in Table 1.

$$C_l = \frac{L}{0.5\rho U_\infty^2 c} \qquad C_d = \frac{D}{0.5\rho U_\infty^2 c} \tag{3}$$

$$\overline{C_l} = \frac{1}{T}\int_0^T C_l(t)dt \qquad \overline{C_d} = \frac{1}{T}\int_0^T C_d(t)dt \tag{4}$$

Table 1- Main airfoil and leading edge device parameters

Parameter	Value	Parameter	Value
Reynolds number(Re)	10 0000	AoA of freestream	5°、15°
chord length(c)	0.1m	pitching amplitude α_m	10°
freestream velocity(U_∞)	15m/s	plunging amplitude h_m	0.5c
turbulence model	SST k-ω	pitching axis location	0.25c
flapping frequency(f)	8Hz	reduced frequency k	0.17

The freestream velocity U_∞ considered herein is 15 m/s, which is close to the cruise speed of the bird. So, the Reynolds number (Re) based on the main airfoil chord length (c) is about 1.0×10^5. To closely simulate the bird flight, the flapping frequency f is selected as 8 Hz to ensure the reduced frequency ($k = \frac{\pi f c}{U_\infty}$) is 0.17.

According to the research and analysis of literature and video[10,11], determine the motion law suitable for this study. Regardless of the flexible deformation of the wing, the influence of geometric parameters of the leading edge device in cruise and take-off and landing States is studied. As shown in Figure 5, the parameters of the leading edge device include diameter(d), distance(l) and deflection angle(θ). By comparing the aerodynamic characteristics of different groups of geometric parameters in the same calculation state, the formation, evolution and shedding process of flow field vortices were observed, the influence of leading edge device on flow field vortices structure was analyzed, and the influence of geometric parameters of leading edge device on wing aerodynamic characteristics was studied. Through comparative analysis, the best geometric parameters of leading edge plume in cruise state and take-off and landing state are obtained.

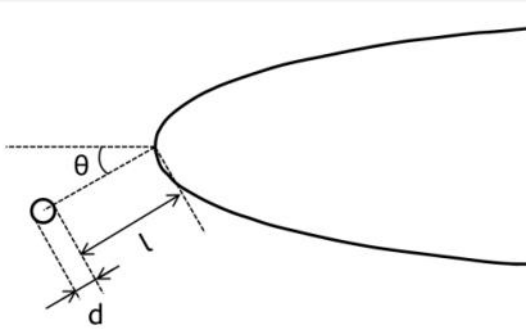

Figure 5 - Geometric parameters of leading edge device

2.2 Numerical method

In this study, commercial software ANSYS fluent is used to simulate the unsteady flow around NACA0012 airfoil and leading edge device. The Reynolds averaged Navier Stokes (RANS) equation was solved to simulate the model. The turbulence model is SST K- ω The numerical method is based on coupled algorithm, and the gradient interpolation method is Least Square Cell Based. The discretization scheme of pressure and momentum is second-order, and the time discretization is first-order implicit. In this paper, the dynamic overset mesh method in fluent is used to realize the pitching and plunging motion of airfoil. The overset mesh is composed of background mesh and component mesh, and the airfoil motion is controlled by user defined function (UDF).

2.2.1 Mesh generation

Firstly, Generate a overset mesh for the NACA0012 airfoil, as shown in Figure 6. Figure (a) is the overall mesh, figure (b) is the component mesh, and figure (c) is the surface mesh of NACA0012 airfoil, in which the height of the first layer mesh is guaranteed to be Y+≤1. As shown in the figure, when arranging the flow field, The distance between the inner flow field boundary and the trailing edge of the airfoil is 6 times the chord length. The distance between the outer flow field boundary along the flow direction and the trailing edge of the airfoil is 31 times the chord length, the distance along the normal direction is 21 times the chord length, and the semicircle radius at the front of the outflow field is 21 times the chord length.The inlet is the boundary condition of velocity inlet, the outlet is the boundary condition of pressure outlet, the outlet pressure is 101325pa, the boundary of overset mesh is the boundary condition of overset, and the airfoil is the boundary condition without sliding wall.

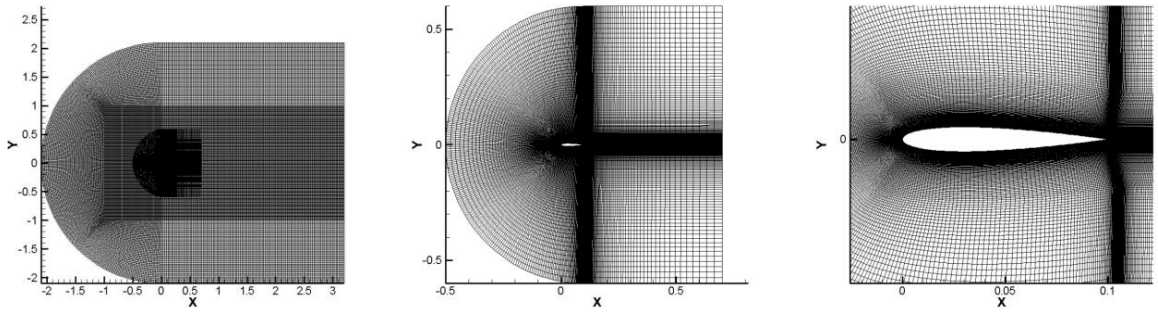

(a)overall mesh (b) component mesh (c) NACA0012 airfoil surface mesh

Figure 6 - NACA0012 airfoil overset mesh

Finally, Generate a overset mesh for the leading edge devices, as shown in Figure 7.The distance between the flow field boundary of the leading edge device mesh and the surface is 5 times the diameter, the boundary is the overset boundary condition. In ANSYS fluent, there are two overset methods for overset mesh, which are density based overset and boundary based overset. This paper adopts the boundary based overset method, and the overset mesh is shown in figure (b).

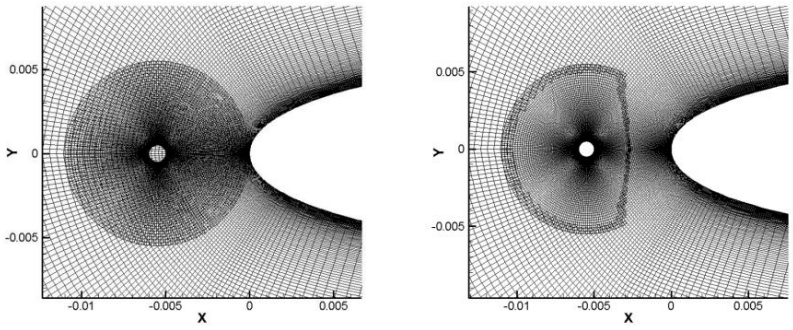

(a) Leading edge device mesh (b) based on boundary overset mesh

Figure 7 - overset mesh of leading edge device

2.2.2 Mesh and time step independence study

In order to select the appropriate calculation parameters and mesh, it is necessary to verify the independence of time step and mesh. In order to get a set of mesh with enough accuracy, the mesh independence verification is carried out. Three groups of different numbers of meshes are selected, and the detailed mesh quantity is shown in Table 2.

Table 2 - Comparison of mesh amount of three groups of meshes

Mesh quantity	background mesh	component mesh	overall mesh
coarse mesh	24224	69258	93482
medium mesh	44659	109198	153857
fine mesh	82361	193678	276039

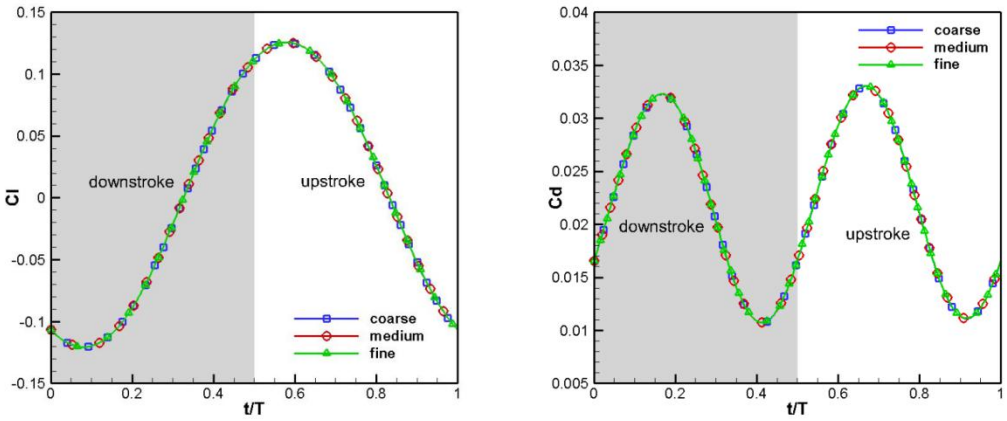

Figure - 8 Comparison of lift coefficient (left) and drag coefficient (right) of different mesh quantities

In mesh independence verification, the calculation parameters in Table 1 are used, and the time step is set to 1250 steps per cycle. Figure 8 shows the comparison of lift coefficient and drag coefficient of different mesh quantity. It can be found that there is no obvious difference in lift coefficient and drag coefficient of three groups of meshes under the same time step. Therefore, medium mesh with 150000 mesh quantity is adopted in the subsequent calculation.

Then, the time step independence is verified to determine how many time steps can be set in each flapping cycle to accurately obtain the force coefficient and flow field structure. Three groups of calculation states are selected, which are 625 steps, 1250 steps and 2500 steps per cycle. The calculation parameters shown in Table 1 are adopted, and the mesh is a medium mesh with 150000 meshes. Figure 9 shows the comparison of lift and drag coefficients in different time steps. It can be found that when 625 steps are calculated in each cycle, the peak value of lift and drag coefficients is slightly different. Under the other two time steps, the lift and drag coefficients are basically consistent. Therefore, 1250 steps per cycle are selected in the subsequent calculation.

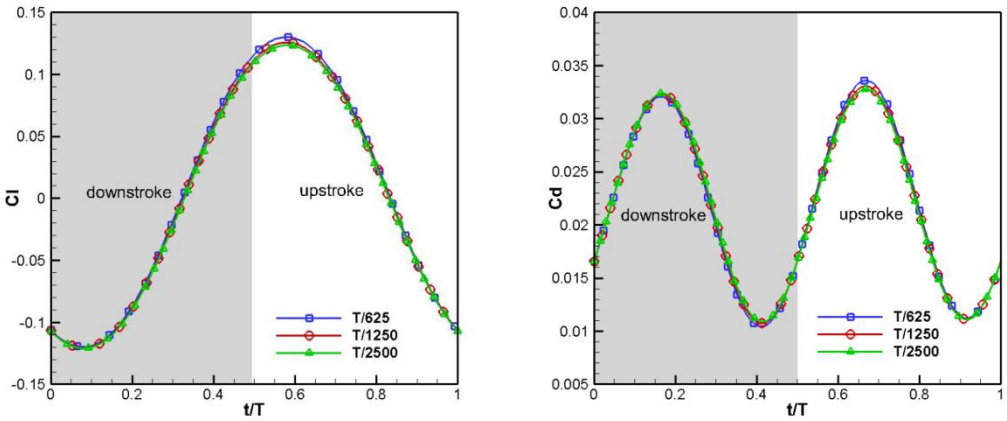

Figure 9 - Comparison of lift coefficient (left) and drag coefficient (right) at different time steps

2.2.3 Numerical validation

In order to verify the effectiveness of this method in calculating the unsteady aerodynamic characteristics of airfoil, we use Mulder's calculation state[8,9]. The pitching and plunging motion of a NACA0012 airfoil is studied in this example. The pitching and plunging motion law is shown in equations 5 and 6. The rotation point of the pitching motion is one third of the chord length from the leading edge of the airfoil.

$$h(t) = h_0 \sin(2\pi f t) \tag{5}$$

$$\theta(t) = \theta_m \sin\left(2\pi f t + \frac{\pi}{2}\right) \tag{6}$$

In the above formula, h is the plunging displacement, the plunging amplitude h_0= c/2, and f is the flapping frequency, θ is the pitching angle, pitching amplitude θ_m=15 °.Relevant calculation parameters are shown in Table 3.

Table 3 - Related calculation parameters in the example of pitching and plunging

Parameter	Value
Reynolds number (Re)	2×10^6
chord length (c)	1m
freestream velocity (U_∞)	29.06m/s
turbulence model	SST k-ω
Flapping period (T)	0.1081s
reduced frequency (k)	1

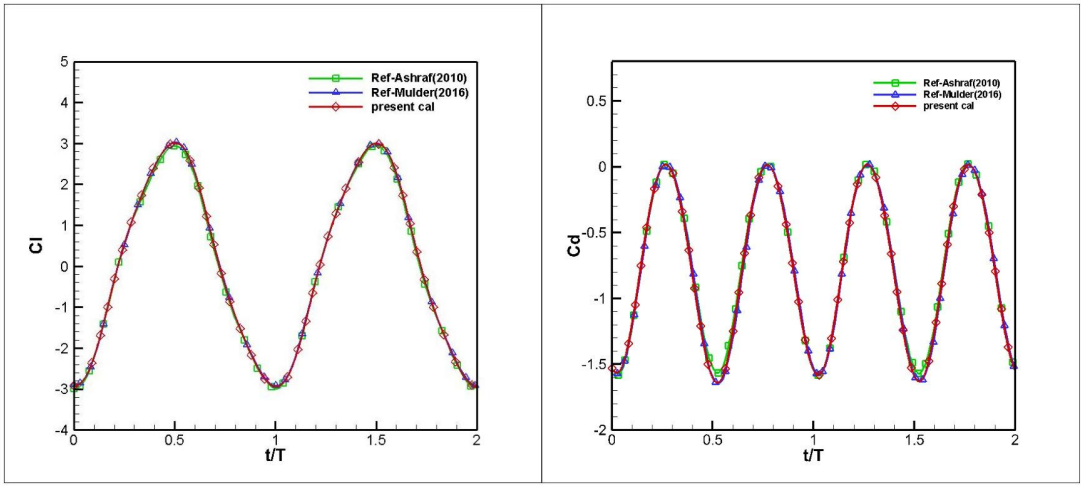

Figure 10 - compare lift coefficient (left) and drag coefficient (right) with references

Comparing the calculation results with those of Mulder and Ashraf, as shown in Figure 10, the left figure shows the comparison of lift coefficient and references, and the right figure shows the comparison of drag coefficient and references. It can be seen that the calculation results of this paper are basically consistent with those of references in the overall trend, peak value and phase, It is proved that the dynamic nested grid method used in this paper is effective and reliable in solving the problems studied in this paper.

3. Results and discussion

In this section, the aerodynamic characteristics of the leading edge device with different geometric parameters (diameter d, distance l) under different deflection angles are studied in detail, and compared with the baseline airfoil without leading edge device. It is known from previous observations that birds only expand the leading edge plume at high angles of attack, such as take-

off and landing. Therefore, the content of this section is divided into two parts 5° And 15 ° The aerodynamic characteristics of the leading edge device under different conditions.

3.1 Calculation results of leading edge device at 5° angle of attack

The calculation results of the leading edge device at an Angle of attack of 5° are shown in Figure 11.The figure shows a comparison of the four leading edge devices with different geometrical parameters to the baseline airfoil (no leading edge devices).Figure(a) shows the variation of the time average lift coefficient with the deflection Angle of the leading device,Figure(b) shows the variation of the time average drag coefficient with the deflection Angle of the leading device, and Figure(c) shows the variation of the time average lift-drag ratio with the deflection Angle of the leading device.The black line is the baseline airfoil, the red line "wire_d1l5" indicates that the leading edge device diameter d is 1mm, and the distance from the leading edge l is 5mm. The other colored lines indicate different diameters and distances.

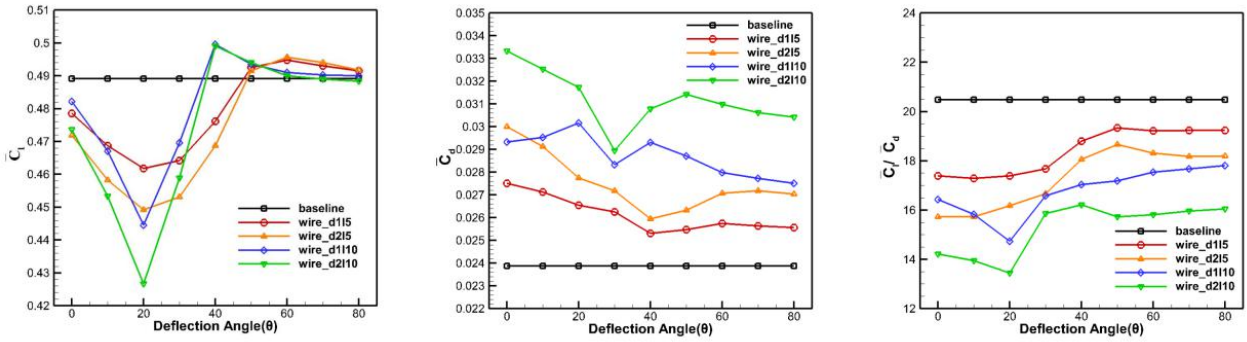

(a) Time average lift coefficient (b) time average drag coefficient (c) time average lift drag ratio

Figure11 - Comparison of leading edge device and baseline airfoil with different geometric parameters at 5° angle of attack

In the case of the same distance (5mm, 10mm), the $\overline{Cl}$、$\overline{Cd}$ and $\overline{Cl}/\overline{Cd}$ variation trends of the leading edge devices with different diameters are the same. The change trend of red line (d1l5) is the same as that of orange line (d2l5), and the change trend of blue line (d1l10) is the same as that of green line (d2l10). When the distance is 5mm, the time average lift coefficient of leading edge devices with diameter of 1mm and 2mm reaches the maximum when the deflection Angle is 60°, and the time average drag coefficient reaches the minimum when the deflection Angle is 40°.When the distance is 10mm, the time average lift coefficient of the leading edge device with diameter of 1mm and 2mm reaches the maximum when the deflection Angle is 40°, and the time average drag coefficient reaches the trough at 40°. It can be seen that the influence of the distance of the leading edge device on the aerodynamic characteristics of the airfoil is greater than that of the diameter of the leading edge device.The time average lift-drag ratio is lower than the baseline airfoil in the 0° to 80° deflection Angle range.It can be found that at an Angle of attack of 5°, the leading edge device will have a negative effect on the aerodynamic characteristics of the airfoil at any deviation Angle.This is consistent with our hypothesis that the leading edge device does not play a positive role at low angles of attack.

3.2 Calculation results of leading edge device at 15° angle of attack

The leading edge coverts of a bird wing only deflects forward at high angles of attack such as take-off and landing, so we study the effects of leading edge devices with different geometric parameters on the aerodynamic characteristics of airfoils at 15° angles of attack.The calculation results of the leading edge device airfoil at an Angle of attack of 15° are shown in Figure12. Figure (a) the variation of the time average lift coefficient with the deflection Angle of the leading edge device, Figure (b) the variation of the time average drag coefficient with the deflection Angle of the leading edge device, and Figure (c) the variation of the time average lift-drag ratio with the deflection Angle of the leading edge device.

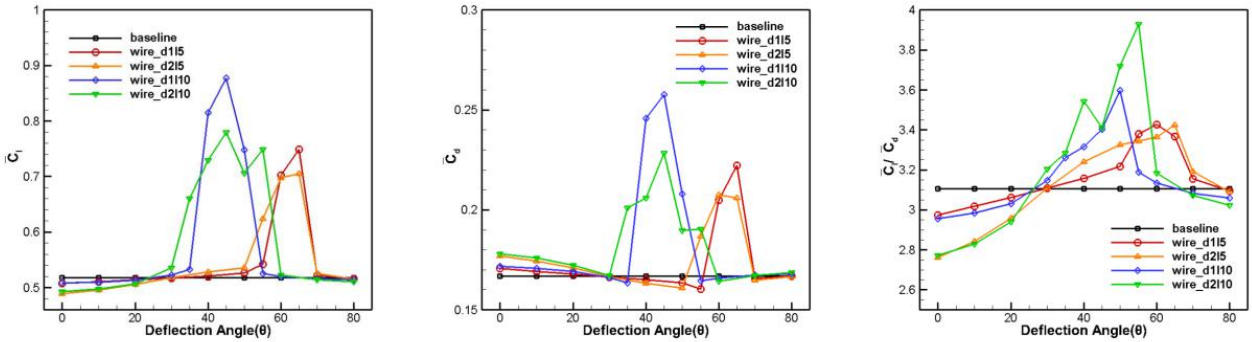

(a)Time average lift coefficient (b) time average drag coefficient (c) time average lift drag ratio

Figure12 - Comparison of leading edge device and baseline airfoil with different geometric parameters at 15° angle of attack

According to Figure12 (a) and (b), a similar result is observed when the Angle of attack is 5°. The influence of the distance between the leading edge device and the leading edge of the airfoil on the aerodynamic characteristics is greater than that of the diameter of the leading edge device on the airfoil.It can be seen from Figure(c) that the time-average lift-drag ratios of these leading edge device airfoils at certain deflection angles are greater than those of the baseline airfoils.Therefore, a leading edge device with a specific deflection Angle at a high Angle of attack will have a positive effect on the aerodynamic characteristics of the airfoil.Moreover, it can be clearly seen from the figure that the leading edge device airfoil with different geometric parameters will generate an unsteady high lift and high drag at certain deflection angles. For example, when the distance is 5mm, both leading edge devices (" wire_d1l5 "and" wire_d2l5 ") will generate a high lift from 50°to 70°.At a distance of 10mm, both leading edge devices (" wire_d1l10 "and" wire_d2l10 ") generate a high lift force between 30°and 60°, and these specific deflection angles are studied in detail below.

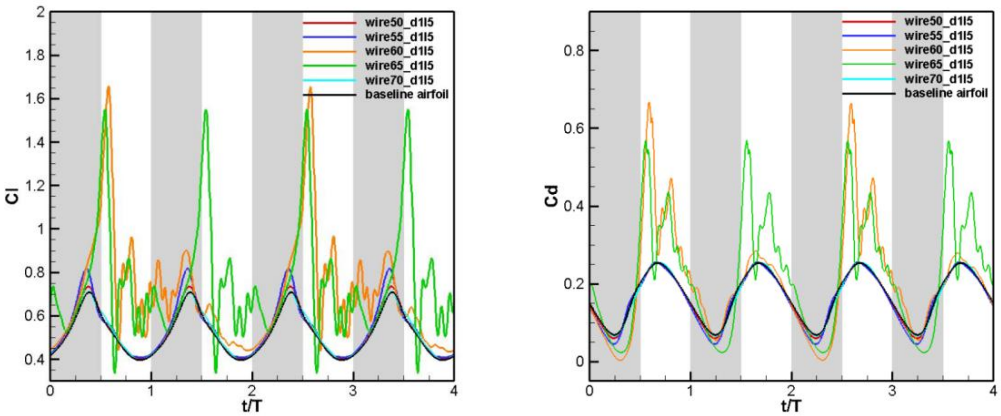

Figure13 - Time histories of lift coefficient (left) and drag coefficient (right) of the leading edge device (" d1l5 ") with deflection Angle of 50° to 70° (gray area is down stroke, white area is up stroke)

Figure13 shows the time histories of lift and drag coefficients of the leading edge device (d=1mm, l =5mm) in four flapping cycles at deflection angles θ=50°, 55°, 60°, 65°, and 70°.In the figure, "wire50_d1l5" represents a leading edge device with diameter d of 1mm, l of 5mm from the leading edge of the airfoil, and deflection Angle θ of 50°.The black line is the baseline airfoil.It can be found that when the deflection Angle of the leading edge device θ=50° and 70°, the lift coefficient of the leading edge device is slightly higher than the baseline airfoil at the peak value, while the drag coefficient is slightly lower than the baseline airfoil at the valley value.The difference is even more pronounced when the deflection Angle θ=55°.When deflection Angle θ=60° and 65°, the leading edge device airfoil will produce an unsteady high lift, and the maximum lift coefficient is much higher than that of the baseline airfoil, and the drag coefficient has the same

trend.In particular, when the deflection Angle θ=60°, the periodicity of the lift coefficient changes, showing the characteristic of one lift coefficient period for every two motion periods.

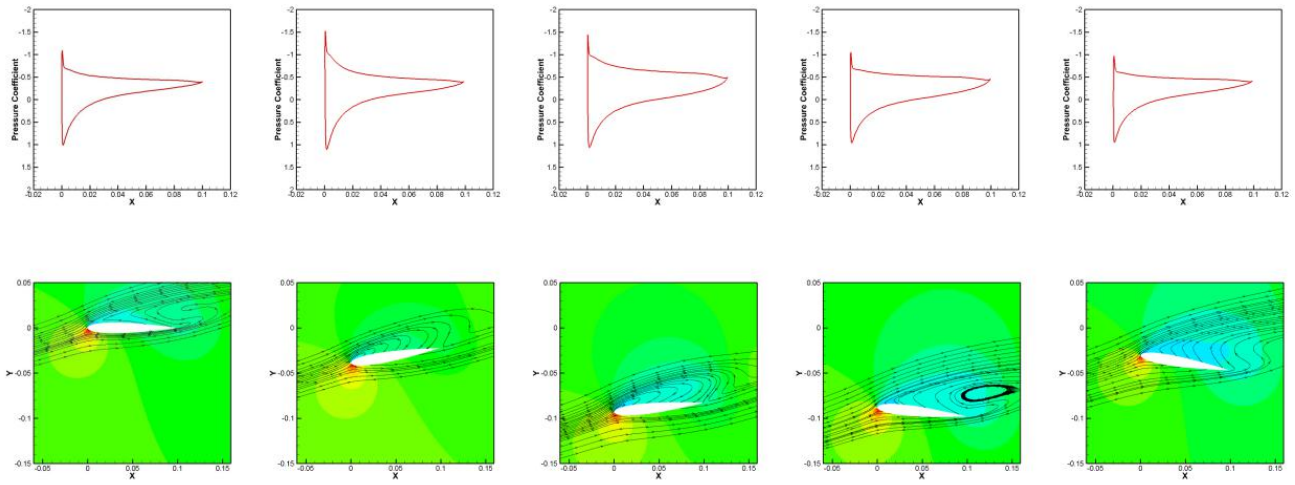

（a）t/T=0　（b）t/T=0.2　（c）t/T=0.4　（d）t/T=0.6　（e）t/T=0.8

Figure14 - Pressure contour(bottom row) and surface pressure coefficient(top row) of the baseline airfoil during one flapping period

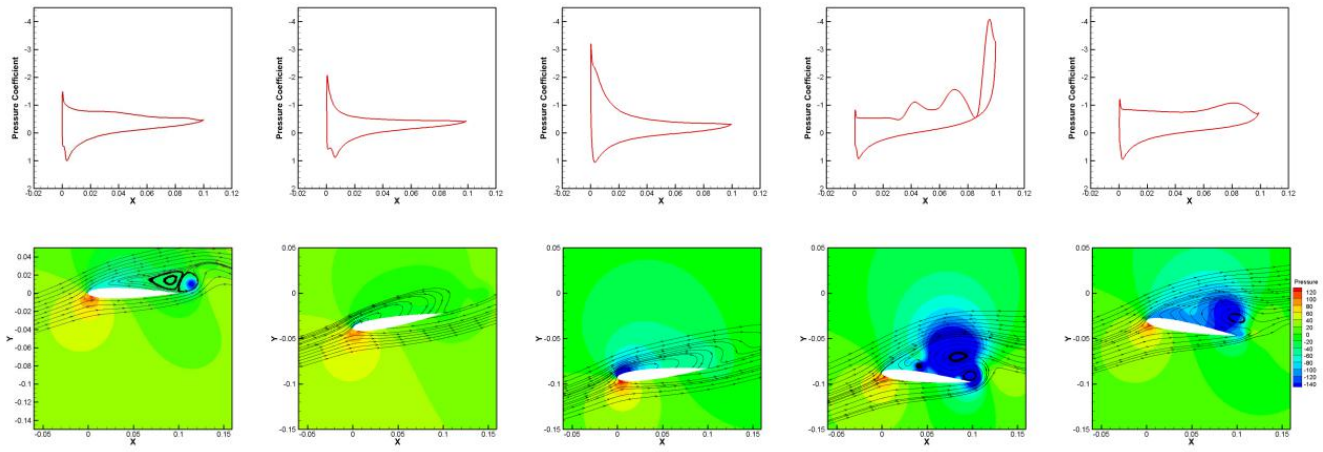

（a）t/T=0　（b）t/T=0.2　（c）t/T=0.4　（d）t/T=0.6　（e）t/T=0.8

Figure15 - Pressure contour,streamline(bottom row) and surface pressure coefficient(top row) of "wire65_d1l5" airfoil in one flapping period

Figures 14 and 15 show the pressure contour ,streamline and surface pressure coefficient of the baseline airfoil and the leading edge device airfoil "wire_d1l5" at different stages of a flapping cycle .It can be found that in all cases, the negative pressure peak of the surface pressure coefficient of the leading edge device airfoil is greater than that of the baseline airfoil.The circular leading edge device will generate a series of vortices similar to Karman vortex street, which will develop downstream and flow to the upper surface of the airfoil at high Angle of attack, resulting in large leading edge vortices during flapping of the airfoil, as shown in Figure15(c).As the leading edge vortex moves to the backward edge and gradually develops into a larger vortex on the upper surface of the airfoil, the negative pressure peak reaches the maximum.This is also the reason why the leading edge device airfoil can produce unsteady high lift at some deflection angles.The time histories of lift coefficient and drag coefficient of other high lift leading edge devices also shows a similar trend.

4. Conclusion

In this study, the bionic leading edge device was numerically simulated, and the aerodynamic characteristics of leading edge devices with different geometric parameters at 5° and 15° angles of attack were compared and analyzed.It can be found that the leading edge device does not have a favorable effect at a small Angle of attack, but produces a very favorable effect at a large Angle of attack.The influence of the distance between the leading edge device and the leading edge on the aerodynamic characteristics of the airfoil is greater than that of the diameter of the leading edge device.At high angles of attack, the leading edge device can generate unsteady high lift, high drag and high lift-to-drag ratio at certain deflection angles, which is also consistent with the previous assumption that the leading edge feather expands during takeoff and landing, and plays a role of increasing lift and drag.

5. Contact Author Email Address

Mail to: gaojiangxin@mail.nwpu.edu.cn

6. Copyright Statement

7. Acknowledgments

This study was supported by the National Natural Science Foundation of China (11872314) and the Key R&D Program in Shaanxi Province of China (2020GY-154).

References

[1] Carruthers A C, Thomas A L R, Taylor G K. Automatic aeroelastic devices in the wings of a steppe eagle Aquila nipalensis[J]. Journal of Experimental Biology, 2007, 210(23): 4136-4149.

[2] Carruthers A, Taylor G, Walker S, et al. Use and function of a leading edge flap on the wings of eagles[C]//45th AIAA Aerospace Sciences Meeting and Exhibit. 2007: 43.

[3] Jones A R, Bakhtian N M, Babinsky H. Low Reynolds number aerodynamics of leading-edge flaps[J]. Journal of Aircraft, 2008, 45(1): 342.

[4] BAKHTIAN, Noel, et al. The low Reynolds number aerodynamics of leading edge flaps. In: 45th AIAA Aerospace Sciences Meeting and Exhibit. 2007. p. 662.

[5] Cojocaru, Marius Gabriel, Mihai Leonida Niculescu, and Claudiu Vadean. "Unsteady numerical estimation of the aerodynamic loads of the Krueger flap." INCAS Bulletin 4.1 (2012): 3.

[6] Shmilovich, Arvin, and Eric D. Dickey. "Leading Edge Devices for Enhanced High-Lift and Reduced Noise." AIAA Scitech 2020 Forum. 2020.

[7] Moffitt, Nicholas J., et al. "Two Approaches to Resolving the Flow Physics of a Krueger Flap for CFD/CAA Analysis." 23rd AIAA/CEAS aeroacoustics conference. 2017.

[8] Ashraf, Muhammad Arif. Numerical simulation of the flow over flapping airfoils in propulsion and power extraction regimes. Diss. University of New South Wales, Australian Defence Force Academy, School of Engineering and Information Technology, 2010.

[9] Hoeijmakers, Harry W., and Joost Mulder. "Computational and experimental investigation into flapping wing propulsion." 54th AIAA aerospace sciences meeting. 2016.

[10] Lee, T., and P. Gerontakos. "Investigation of flow over an oscillating airfoil." Journal of Fluid Mechanics 512 (2004): 313.

[11] Gharali, Kobra, and David A. Johnson. "Dynamic stall simulation of a pitching airfoil under unsteady freestream velocity." Journal of Fluids and Structures 42 (2013): 228-244.